analytical chemistry

Article

pubs.acs.org/ac

Fluorescence Quenching of Graphene Oxide Integrating with the Site-Specific Cleavage of the Endonuclease for Sensitive and Selective MicroRNA Detection

Yunqiu Tu, Wen Li, Ping Wu,* Hui Zhang, and Chenxin Cai*

Jiangsu Key Laboratory of New Power Batteries, College of Chemistry and Materials Science, Nanjing Normal University, Nanjing 210097, People's Republic of China

Supporting Information

ABSTRACT: A considerable effort is currently focused on identifying microRNA (miRNA) biomarkers because they could serve for early disease diagnosis as well as for assessing the prognosis and monitoring the response to treatment. The efficient use of the biomarkers requires precise analysis of miRNAs. This work reports a rapid, sensitive, and selective miRNA assay by coupling the fluorescence quenching of graphene oxide (GO) with site-specific cleavage of an endonuclease. The method is developed by designing a single-stranded probe that carries both a binding region responsible for facilitating the interaction with GO, which induces fluorescence quenching of the 5′-terminus-labeled fluorophore (FAM, 6-carboxyfluorescein), and a sensing region for specifically recognizing the target and hybridizing with it to form a duplex. The duplex is released from the GO surface through cleavage of *Rsa*I endonuclease, resulting in fluorescence recovery, which shows a trend in the target concentration. The assay can detect down to ~3.0 fM miR-126 with a linear range of 4 orders of magnitude and has an ability to discriminate the target sequence from even single-base mismatched sequence or other miRNA sequences. Moreover, it can also be used for estimating the miR-126 expressions in cells. The advantage of this assay is that it operates via the detection of the recovered fluorescence signal, which is a combined result of the specific hybridization and the site-specific cleavage, and thus should be impervious to false signals arising due to the nonspecific adsorption of interferants. It could be a great potential tool for selective analysis of miRNAs in cells.

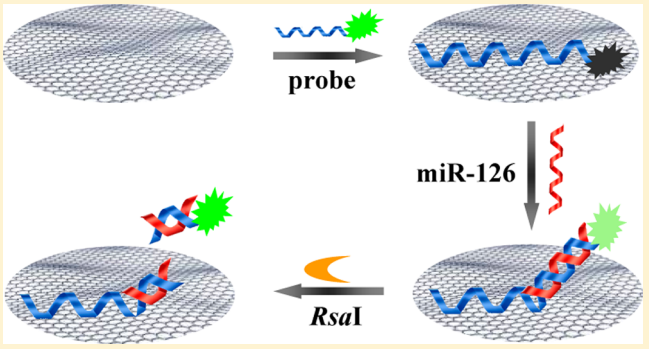

MicroRNAs (miRNAs) are a family of small noncoding 18−25 nucleotide long RNAs expressed in many organisms including animals, plants, and viruses.[1,2] In these organisms, miRNAs regulate the gene expression by complementary binding to the 3′-untranslated regions of their target mRNAs that either leads to mRNA degradation or translational repression, depending on the degree of complementary sequences between the miRNAs and their targets.[3,4] Recent studies have showed that miRNAs also play important roles in a wide range of physiological and pathological events (including cell development, differentiation, metabolism, and apoptosis)[5,6] and cancer development and progression in particular.[7−11] Cancer-specific miRNA fingerprints have been identified in many types of analyzed cancers (including breast carcinoma, primary glioblastoma, hepatocellular carcinoma, and lung cancer).[9,12−14] The unique patterns of miRNA expression in cancer cells could serve as a diagnostic fingerprint.[12,14] Therefore, miRNAs may be good biomarkers for diagnosis, prognosis, and prediction of cancer, and they may even be targets for new drug discovery.[14−16]

The efficient use of a miRNA biomarker requires precise analysis of miRNAs. However, small size, high sequence homology among family members, low abundance, susceptibility to degradation, and common secondary structures of miRNAs have complicated efforts to develop accurate, unbiased quantification techniques.[17−20] The most popular and well-established miRNA profiling methods are adapted from traditional nucleic acid analysis techniques. Northern blotting,[21] microarray analysis,[22] and real-time quantitative polymerase chain reaction (qRT-PCR)[23,24] are current widely used standard methods for miRNA analysis. However, these methods have some limitations.[25] For example, the northern blotting assay is time-consuming with moderate sensitivity and low throughput and usually requires large amounts of samples (often more than 1 μg of total RNA), which limits its application in clinical diagnosis.[26] Microarray analysis requires preamplification, which yields significant sequence bias, and suffers from cross hybridization and poor reproducibility.[27] Although qRT-PCR has the advantages of practical ease, high sensitivity, and accuracy, the short length of miRNA

Received: December 26, 2012
Accepted: January 15, 2013
Published: January 15, 2013

   dx.doi.org/10.1021/ac303772m | *Anal. Chem.* 2013, 85, 2536−2542

sophisticates the design of the primers, for example, the stem-loop primer and the locked nucleic acid (LNA)-modified primer, increasing the experimental cost and complexity.[24] Moreover, qRT-PCR requires the precise control of temperature cycling for successful amplification, which increases the analysis difficulty.[28] In addition, these assay technologies are expensive and require well-trained scientists.

Recently, several new miRNA detection methods based on integration of the unique optical, electronic, and catalytic characteristics of nanomaterials with highly specific recognition ability of biomolecules were reported.[29−37] However, some of these methods require a chemical or enzymatic modification of target miRNA prior to the analysis or the application of LNAs as capture probes owing to the short length of miRNAs. Modifications make the analysis cumbersome and lead to reduced accuracy due to different efficiencies of modifications for different miRNAs.

Novel and improved techniques for detection and quantification of miRNAs are currently essential to unravel the functions and mode of actions of these small molecules and are therefore urgently needed. This work reports a rapid, sensitive, and selective miRNA assay by coupling the fluorescence quenching graphene oxide (GO) with site-specific cleavage of an endonuclease for improving selectivity (Figure 1). We designed a single-stranded probe DNA that carries both a binding region (44 bases) and a sensing region (22 bases). The binding region provides an anchoring function to facilitate the interaction between GO and the probe, inducing fluorescence quenching of the 5′-terminus-labeled fluorophore (FAM, 6-carboxyfluorescein). The sensing region specifically recognizes the target miRNA (miR-126; we selected miR-126 as the assay target due to its importance in preventing growth of many cancers, such as primary bladder, prostate, colorectal, gastric, human breast, and lung cancers.[9,11,12] In addition, the expression and roles of miR-126 may be different in various malignancies, and therefore, it can be used as a biomarker for many cancers.[7]) and hybridizes with it to form a duplex, which contains the specific sequence recognized by *Rsa*I endonuclease (a site-specific endonuclease recognizing the duplex symmetrical tetranucleotide sequence 5′-GTAC-3′ and catalyzing cleavage between T and A bases[38]). In the absence of a specific target, no fluorescence signal is detected. In the presence of a miRNA target, however, the formed duplex is subject to be released from the GO surface under the cleavage of *Rsa*I endonuclease, resulting in the recovery of fluorescence of the fluorophore and producing a readily detectable signal. The degree of recovery of the fluorescence signal shows a trend in target miRNA concentration in solution, which establishes the basis of the quantitative detection of miRNA. The extraordinarily high quenching efficiency of GO (resulting in a high signal-to-background ratio) and the high site-specific cleavage of *Rsa*I endonuclease (resulting a high selectivity) make the present method a promising assay for miRNA with high sensitivity and selectivity.

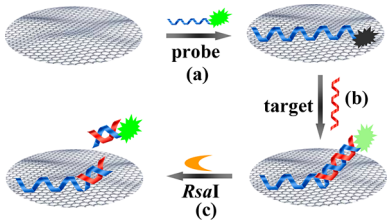

Figure 1. Illustration of miRNA assay based on coupling the fluorescence quenching of GO with site-specific cleavage of an endonuclease. The designed P1, which is labeled at its 5′-terminus with a fluorophore, exhibits partial complementarity to the target (T1). The adsorption of P1 on the GO surface effectively quenches the fluorophore (step a). The hybridization of P1 with T1 leads to a non-GO absorbed duplex region and a single-stranded domain that is associated with the GO surface (step b). In the presence of the endonuclease, the 5′-terminus of the duplex (containing the *Rsa*I-recognized tetranucleotide sequence 5′-GTAC-3′) is digested, resulting in the release of the fluorophore to the solution and recovery of the fluorescence signal (step c). The recovered fluorescence signal depends on the target concentration in solution.

EXPERIMENTAL SECTION

Chemicals. Graphite powder (99.998%, 325 mesh) was from Alfa Aesar; 4-(2-hydroxyethyl)-1-piperazineethanesulfonic acid (HEPES), 1,4-dithiothreitol (DTT), tris(hydroxymethyl)-aminomethane (Tris), and bovine serum albumin (BSA) were from Sigma−Aldrich and used as received. 1X NEBuffer 4 solution (20 mM Tris−acetate, 50 mM potassium acetate, 10 mM magnesium acetate, and 1 mM DTT, pH 7.9) and *Escherichia coli* restriction endonuclease *Rsa*I were purchased from New England BioLabs. The *Rsa*I endonuclease was stored in 10 mM Tris−HCl (pH 7.4) containing 100 mM NaCl, 1 mM DTT, 0.1 mM EDTA, 200 μg/mL BSA, and 50% (v/v) glycerol. All solutions were prepared with doubly distilled water.

The oligonucleotides were purchased from BioSune Biological Engineering Technology Co. (Shanghai, China). The nucleic acids were purified by high-performance liquid chromatography and freeze-dried. The sequences of the oligonucleotides were summarized in Table 1.

Preparation of GO. GO was prepared by a modified Hummers method,[39,40] starting from graphite powder (99.998%, 325 mesh). The detailed procedures have been reported in our previous works.[41,42] The prepared GO sheets are rippled and resemble crumpled silk veil waves (transmission electron microscopy image in Figure S1a of the Supporting Information) with thickness of ∼0.8 nm (atomic force microscopy image in Figure S1b of the Supporting Information). The Fourier transform IR spectrum exhibits the characteristic vibrations of GO (Figure S1c, Supporting Information), including the stretching mode of O—H (∼3440 cm^{-1}), the stretching vibrations of C═O (1750 cm^{-1}), sp^2 hybridized C═C (1640 cm^{-1}), and C—OH groups (1233 cm^{-1}), and the deformation mode of C—O groups (1060 cm^{-1}).[43] The GO has a C/O ratio of ∼1.8, which was estimated by integrating the C1s peak at 284.6 eV and the O1s peak at 532.7 eV in the X-ray photoelectron spectrum (Figure S1d, Supporting Information). Deconvoluting the C1s peak shows that this peak contains C—C (∼284.6 eV), C—O (∼286.8 eV), C═O (∼287.6 eV), and O—C═O (∼288.9 eV) elements[44] (Figure S1e, Supporting Information). These results suggest that the single layer GO has been synthesized in our experimental conditions.

Fluorescent miRNA Assays. Fluorescence spectra were collected with a Cary Eclipse fluorescence spectrophotometer (Varian) equipped with a xenon lamp excitation source. The FAM was excited at 494 nm, and the fluorescence emission spectra were recorded from 510 to 700 nm. The measurements were performed in 1X NEBuffer 4 solution at 37 °C and pH 7.9. In a typical assay, 10 μL of GO dispersion (100 μg/mL)

dx.doi.org/10.1021/ac303772m | *Anal. Chem.* 2013, 85, 2536−2542

Table 1. Sequences of Oligonucleotides Used in This Work

description	sequence
66-base FAM-labeled single-stranded probe DNA (P1). The underlined bases are responsible for hybridizing with target. Note that, to retain the duplex of the target and the FAM-labeled P1 on the GO surface, the binding region of P1 was designed to have two times as many bases of that in sensing region.	5′-FAM-TCG TAC CGT GAG TAA TAA TGC GAG CTA TGT GCC GAA TAT CAA GGA CAG TTG TAG CTA TGT GCC GAA-3′
22-base miR-126 cDNA (T1, perfect matched target)	5′-C GCA TTA TTA CTC ACG GTA CGA-3′
22-base modified miR-126 cDNA (T2, one-base mismatch. The mismatched base is out of the *Rsa*I-recognized sequence.)	5′-C GAA TTA TTA CTC ACG GTA CGA-3′
22-base modified miR-126 cDNA (T3, two-base mismatch. The mismatched bases are out of the *Rsa*I-recognized sequence.)	5′-C GAA TTA TAA CTC ACG GTA CGA-3′
22-base modified miR-126 cDNA (T4, three-base mismatch. The mismatched bases are out of the *Rsa*I-recognized sequence.)	5′-C GAA TTA TAA CTC AAG GTA CGA-3′
22-base modified miR-126 cDNA (T5, one-base mismatch. The mismatched base locates in the *Rsa*I-recognized sequence.)	5′-C GCA TTA TTA CTC ACG GAA CGA-3′
22-base miR-141 cDNA	5′-C CAT CTT TAC CAG ACA GTG TTA-3′
22-base miR-21 cDNA	5′-T CAA CAT CAG TCT GAT AAG CTA-3′
22-base let-7a cDNA	5′-A ACT ATG CAA CCT ACT ACC TCT-3′
23-base miR-122 cDNA	5′-AC AAA CAC CAT TGT CAC ACT CCA-3′

and 1 μL of FAM-labeled DNA (P1, 1 μM) were mixed together and diluted to 100 μL using 1X NEBuffer 4 solution (step a in Figure 1). After a stable background fluorescence of the solution was attained, different concentrations of the target were added to the solution and allowed to hybridize with P1 for 1 h (step b in Figure 1), which is long enough to ensure the complete hybridization. Then, *Rsa*I was added to the system with the final concentration of 0.2 U/mL, and the time-dependent fluorescence changes of the FAM were monitored (step c in Figure 1).

Cell Culture. H226 (human mesothelioma cell), A549 (human adenocarcinoma cell), H358 (transformed human bronchoalveolar cell), and MDA-MB231 (human breast cancer cell) cell lines were obtained from the cell bank of type culture collection of the Chinese Academy of Sciences (Shanghai, China) and cultured at 37 °C in RPMI 1640 medium supplemented with 10% fetal bovine serum (FBS), 2 mM L-glutamine, 100 U/mL penicillin, and 100 μg/mL streptomycin in a 5% CO_2 environment. HMVEC cells (human microvascular endothelial cell, PromoCell, Heidelberg, Germany) were cultured in endothelial cell growth medium (EGM2-MV medium) containing 2% FBS at 37 °C with humidified 95% air containing 5% CO_2. MCF-10A cells (human normal breast epithelial cells, ATCC) were cultured in DMEM/F-12 medium containing 5% horse serum, 100 U/mL penicillin, 100 mg/mL streptomycin, 100 ng/mL cholera toxin, 10 ng/mL epidermal growth factor, 0.5 mg/mL hydrocortisone, 10 mg/mL insulin, and 1% L-glutamine at 37 °C under an atmosphere of 5% CO_2. After growing to 90% confluence, the cells were washed with phosphate-buffered saline (PBS; 0.145 M NaCl, 1.9 mM NaH_2PO_4, 8.1 mM K_2HPO_4, pH 7.4), the culture medium was replaced by 1 mL of PBS, and the cell number was estimated by a hemocytometer.

Preparation of Cellular Extracts. The preparation of cellular extracts was conducted according to a reported method.[30] Briefly, ~10^7 cells were washed once with PBS and twice with buffer A (10 mM HEPES, pH 7.9 at 4 °C, 1.5 mM $Mg(NO_3)_2$, 10 mM KNO_3, and 0.5 mM DTT). The cell pellet was suspended in buffer B (20 mM HEPES (pH 7.9), 25% (v/v) glycerol, 0.42 M $NaNO_3$, 1.5 mM $Mg(NO_3)_2$, 0.2 mM EDTA, 0.5 mM phenylmethylsulfonyl fluoride (PMSF), and 0.5 mM DTT)/0.1% Nonidet P-40 (20 μL). After incubating for 15 min on ice, the lysed cellular suspension was briefly mixed on a vortex and microcentrifuged for 10 min at 4 °C. The supernatant was diluted with 80 μL of buffer C (20 mM HEPES (pH 7.9), 20% (v/v) glycerol, 0.1 M KNO_3, 0.2 mM EDTA, 0.5 mM PMSF, and 0.5 mM DTT) and stored at −80 °C. The RNA was routinely assessed by gel electrophoresis and UV−visible spectrophotometry following reported procedures.[45] The samples of cDNA were obtained by nested reverse transcription polymerase chain reaction (RT-PCR).

RESULTS AND DISCUSSION

We first evaluated the fluorescence quenching ability of GO by examining the change of fluorescent signal of FAM-labled P1 in the presence of GO. In the absence of GO in the solution, P1 exhibits a strong characteristic fluorescence signal of FAM at ~520 nm[31,46] (curve a in Figure 2A). Upon the addition of GO into solution, we found that the fluorescence of FAM was rapidly quenched by GO in a GO concentration-dependent manner (curves b−g in Figure 2A and the inset). Note that the fluorescence signals of GO do not affect the fluorescence features of FAM because the fluorescence signals of GO alone are very low under our experimental conditions (curve h in Figure 2A). The fluorescence spectra of GO at different concentrations (0−12 μg/mL) are depicted in Figure S2 of the Supporting Information. The fluorescence intensity of FAM decreased with the increase of the GO concentration (the concentration of P1 was kept at 10 nM) and was almost

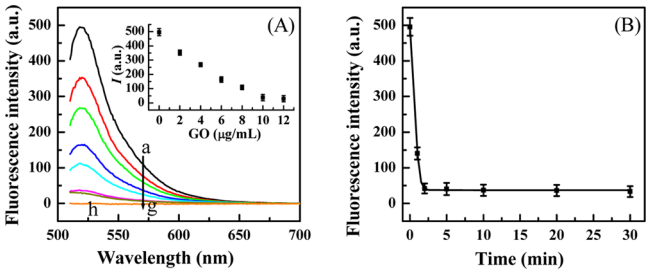

Figure 2. (A) Fluorescence quenching of FAM-labeled P1 (10 nM) at the GO surface with GO concentrations of (a−g) 0, 2, 4, 6, 8, 10, and 12 μg/mL. Curve h shows the fluorescence emission spectra of GO alone at a concentration of 12 μg/mL. The inset shows the dependence of the fluorescence intensity at 520 nm on the GO concentration. (B) Time-dependent fluorescence changes of P1 (10 nM) quenched by GO (10 μg/mL). Error bars were based on five measurements.

dx.doi.org/10.1021/ac303772m | *Anal. Chem.* 2013, 85, 2536−2542

completely quenched at GO concentration of 10 μg/mL (the inset of Figure 2A), indicating good fluorescence quenching ability of our prepared GO. Kinetic studies showed that the fluorescence quenching of GO is fairly fast because the fluorescence intensity decreased rapidly to ∼28% of the initial intensity in ∼1 min and was completely quenched within 2 min (Figure 2B). However, no time-dependent fluorescence changes were observed for P1 in solution in the absence of GO (not shown here), implying that the time-dependent changes depicted in Figure 2B originate from the fluorescence quenching of GO. The good quenching ability of GO possibly arose from the strong hydrophobic adsorption of P1 at the GO surface and highly efficient long-range energy transfer from FAM to GO.[47−49]

Next, we studied the fluorescence recovery of the completely quenched FAM-labeled P1 upon the addition of the target and *Rsa*I endonuclease into the system. Introducing the target (T1, 10 pM) into the solution results in a slight recovery of the fluorescence intensity of the quenched FAM (curve b in Figure 3A). For better comparison, the fluorescence spectrum of P1 on the GO surface was also depicted in Figure 3A, curve a. This is attributed to T1 hybridizing with P1 to form the duplex P1/T1, leading the FAM label to be away from the GO surface due to the weaker interaction between GO and the duplex caused by the shielding affects of nucleobases within the double-helix structure.[48,50] However, the enhanced fluorescence intensity is still very low, implying that nearly no P1 is released to the solution. Otherwise, the fluorescence will be fully recovered. The duplex on the GO surface is stable because its fluorescence intensity has only a minute change in 3 h (Figure S3, Supporting Information). Note that, to retain the duplex of the target and the FAM-labeled P1 on the GO surface stably, the number of the bases in the binding region of the probe should be at least 1−2 times of that in its sensing region.[49] The numbers of bases in the binding and sensing regions of our designed probe P1 are 44 and 22, respectively. The fluorescence intensity can be greatly recovered by adding *Rsa*I endonuclease to the solution (0.2 U/mL) (curve c in Figure 3A) because *Rsa*I cleaved the duplex (P1/T1) between the bases T and A in the 5′-GTAC-3′ sequence and released FAM into the solution. The fluorescence intensity increases further with prolonged cleavage time (curves d−h in Figure 3A) and tends to be saturated after 2 h (the inset of Figure 3A) because almost all of the P1/T1 duplex at the GO surface has been cleaved by *Rsa*I endonuclease and released into solution. The fluorescence intensity of FAM also depends on the amount of endonuclease added to the solution. It rises with the increase of the concentration of endonuclease in solution and reaches a relative stable value when the endonuclease concentration is higher than 0.2 U/mL (2 h cleavage) (Figure 3B).

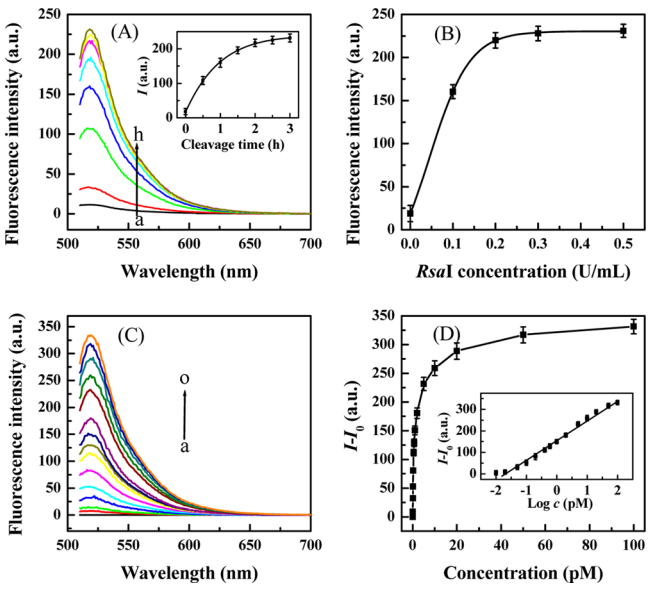

Figure 3. (A) Fluorescence spectra of the P1/T1 duplex at the GO surface after cleavage by *Rsa*I endonuclease for (b−h) 0, 0.5, 1.0, 1.5, 2.0, 2.5, and 3.0 h, respectively. Curve (a) depicts the fluorescence spectrum of FAM-labeled P1 at the GO surface. The inset shows the dependence of the fluorescence intensity of the duplex on the cleavage time. The concentration of *Rsa*I in solution is 0.2 U/mL. (B) Dependence of the fluorescence intensity on *Rsa*I concentration. The cleavage time for each *Rsa*I concentration was 2 h. (C) The background-subtracted fluorescence spectra of the P1/T1 duplex after 2 h cleavage with the endonuclease (0.2 U/mL). The duplex was formed by hybridizing P1 at the GO surface with (a−o) 0, 0.01, 0.02, 0.05, 0.1, 0.2, 0.4, 0.6, 1.0, 2.0, 5.0, 10, 20, 50, and 100 pM T1, respectively. (D) Dependence of the background-subtracted fluorescence intensity ($I - I_0$) on the target concentration. The data were acquired from panel C. The inset shows the plot of ($I - I_0$) vs the logarithm of the target concentration. I is the fluorescence intensity of the system at the respective concentrations of the target, and I_0 corresponds to the fluorescence intensity of the system in the absence of both the target and *Rsa*I endonuclease. Error bars were based on five measurements.

To validate the observed fluorescence recovery ascribed to the release of the FAM fluorophore from the GO surface caused by cleaving the P1/T1 duplex with *Rsa*I endonuclease, three control experiments were further designed and performed. One control was made by cleaving the P1/T1 duplex with *Rsa*I endonuclease in buffer conditions without Mg^{2+} ions, since *Rsa*I endonuclease is a Mg^{2+}-dependent glycoprotein and requires Mg^{2+} ions to be activated.[38] As shown in Figure S4 of the Supporting Information, the fluorescence of the P1/T1 duplex does not increase after 2 h cleavage with *Rsa*I as the endonuclease does not work effectively in the absence of Mg^{2+} ions (Figure S4a, Supporting Information). The second control was made by heating the *Rsa*I endonuclease at 90 °C for 10 min to undergo an irreversible inactivation. We find that the activity of heat-treated *Rsa*I endonuclease is reduced greatly because the fluorescence intensities are not observed to increase upon the 2 h cleavage of the inactivated *Rsa*I endonuclease (Figure S4b, Supporting Information). The third control was made by recording the fluorescence changes of the P1-functionalized GO with cleavage of *Rsa*I endonuclease (2 h) in the absence of the target T1. The results indicate that the interaction of P1 with *Rsa*I causes almost no fluorescence change in the solution (Figure S4c, Supporting Information). These results confirm that the observed fluorescence recovery depicted in Figure 3A originates only from the cleavage of the resulting P1/T1 duplex with *Rsa*I endonuclease.

The recovery of the fluorescence intensity also depends on target (T1) concentrations. The intensity increases with the concentration of T1 in solution (Figure 3C) at lower concentration and then levels off at higher concentration (Figure 3D). The plot of the background-subtracted fluorescence intensity versus the logarithm value of T1 concentration displays a linear relationship in the range from 0.02 to 100 pM with a limit of detection (LOD) of ∼3.0 fM (at

dx.doi.org/10.1021/ac303772m | *Anal. Chem.* 2013, 85, 2536−2542

a signal/noise of 3) (inset, Figure 3D). Although the LOD value is much higher than that obtained based on target-assisted isothermal exponential amplification coupled with fluorescent DNA-scaffolded silver nanocluster (~2 aM),[30] it is comparable with the miRNA detection method based on the GO fluorescence quenching combined with the isothermal strand-displacement polymerase reaction (2.1 fM)[31] and is superior to the GO-based premixing detection system (100 pM).[48] Meanwhile, the LOD is competitive with other sensitive miRNA detection strategies.[18,32] A series of 10 repetitive measurements with 10 pM T1 was used for evaluating the precision of the proposed method, and a relative standard deviation (RSD) of ~3.5% was obtained, demonstrating good reproducibility of the assay. These results indicate that the proposed method can be used for the sensitive miR-126 assay.

Having studied fluorescence recovery of the quenched FAM-labeled P1 at the GO surface by the hybridization with the target and cleavage by *Rsa*I endonuclease, we evaluated the selectivity of the proposed method toward the detection of miR-126. We designed four kinds of mismatched target sequences including a single-base (T2, the mismatched base is out of the *Rsa*I-recognized sequence; T5 the mismatched base is in the *Rsa*I-recognized sequence), two-base (T3), and three-base (T4) mismatched targets (refer to Table 1 for the sequences of these mismatched targets). After FAM-labeled P1 was hybridized with the respective mismatched target at the GO surface for 1 h and then cleaved by 0.2 U/mL *Rsa*I for 2 h, the fluorescence spectra were recorded, and the fluorescence intensities at 520 nm were compared with that obtained with perfect matched target (T1). As shown in Figure 4A, the

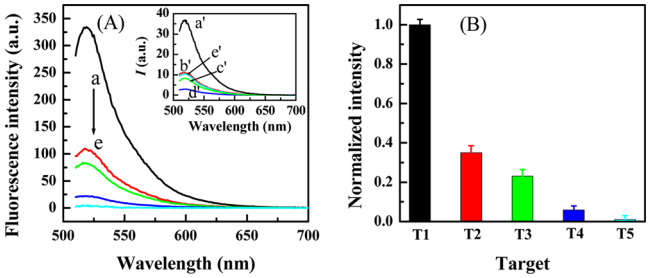

Figure 4. (A) Background-subtracted fluorescence spectra of FAM-labeled P1 at the GO surface after hybridization with 10 pM of (a) perfect matched (T1), (b) single-base (T2, the mismatched base is out of the *Rsa*I-recognized sequence), (c) two-base (T3), (d) three-base (T4), and (e) single-base mismatched targets (T5, the mismatched base is in the *Rsa*I-recognized sequence), respectively, and 2 h cleavage by *Rsa*I endonuclease (0.2 U/mL). (B) Dependence of the normalized fluorescence intensity on the number of mismatched bases in the target sequence. Inset in panel A shows fluorescence emission spectra of the duplex of 1 nM FAM-labeled P1 at the GO surface with 10 pM of (a′) T1, (b′) T2, (c′) T3, (d′) T4, and (e′) T5, respectively (without cleavage by *Rsa*I endonuclease). Error bars were based on five measurements.

proposed assay displays high sequence specificity to discriminate the perfectly complementary target from even single-base mismatched strands. The fluorescence intensities (note that the spectra in Figure 4A have been corrected with respective background, which were shown in the inset. The background referred to the spectrum of the duplex of the FAM-labeled P1 with the correspondent mismatched target without the cleavage of *Rsa*I) for T2, T3, and T4 were ~35%, 23%, and 6%, respectively, of that for the perfect matched T1 target (curves a–d in Figure 4A and also refer to Figure 4B). For T5, almost no fluorescence intensity change could be detected before and after the cleavage by *Rsa*I endonuclease (curve e in Figure 4A and Figure 4B) because *Rsa*I cannot cleave the P1/T5 duplex due to a mismatched base in the *Rsa*I-recognized sequence. These results suggest that the proposed approach with high sequence specificity has a potential application in single nucleotide polymorphism analysis.

The sequence specificity of the assay was further evaluated by four artificially synthesized cDNAs of miR-141 (up-expressed in prostate cancer cells, AsPc-1), miR-21 (highly expressed in human breast cancer cells, MD-MB231), let-7d (conservative among human cells), and miR-122 (specifically expresses in the liver and is an important component of gene regulatory networks in the liver for normal hepatocyte function, playing a key role in the regulation of hepatitis C virus replication[51]). For better comparison, the FAM-labeled P1 at the GO surface was hybridized for 1 h with the cDNA of miR-141, miR-21, let-7d, and miR-122 (each at the concentration of 10 pM), respectively, and then was cleaved by 0.2 U/mL *Rsa*I endonuclease for 2 h. After that, the fluorescence signal was recorded. We find that there is nearly negligible fluorescent change in the presence of the cDNA of miR-141, miR-21, let-7d, and miR-122 (not shown here), confirming that the specificity of the method is high enough to discriminate the specific target from the different types of miRNAs and shows the significant advantage of high selectivity.

We finally applied the developed method to estimate miR-126 relative expressions in several different types of cells. We prepared a primary cell lysate sample (HMVEC) and three lung cancer cell lysate samples (H226, A549, and H358). The expressions of miR-126 in four different cell lysate samples were estimated by the proposed method. As depicted in Figure 5, the expression of miR-126 in H226, A549, and H358 is much lower than that in HMVEC and has only ~15%, 6%, and 5%, respectively, of that in HMVEC (note that the expressions of miR-126 in H226, A549, and H358 cells were normalized with

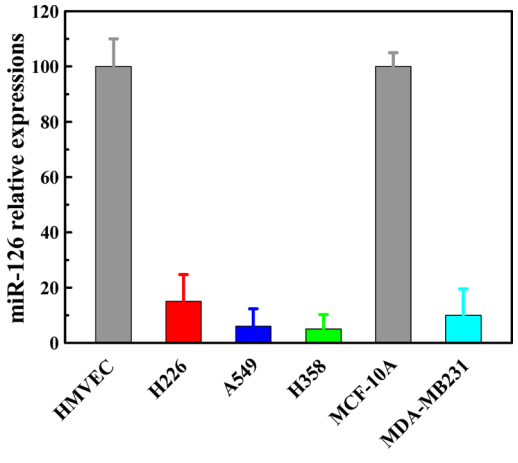

Figure 5. Estimation of the miR-126 relative expressions in different types of cells using the developed method. The expression of miR-126 in H226, A549, and H358 cells was normalized with that in HMVEC cells. We obtained the normalized values by comparing the respective fluorescence intensities of H226, A549, and H358 cell lysates with that of HMVEC cells. The expression of miR-126 in MDA-MB231 cells was normalized with that in MCF-10A cells. The value was obtained by comparing the fluorescence intensities of MDA-MB231 cells with that from MCF-10A cells. Error bars were based on five experiments.

dx.doi.org/10.1021/ac303772m | *Anal. Chem.* 2013, 85, 2536–2542

that in the HMVEC cells), agreeing well with those obtained from RT-PCR and the northern blotting assay.[12] This conclusion is also consistant with those reports[10,13] that the decrease in miR-126 expression can lead to the development of lung cancer.

We also prepared the cell lysate samples of human normal breast epithelial cells (MCF-10A) and human breast cancer cells (MDA-MB231), and the miR-126 expression levels in these cells were estimated using the developed method to further evaluate the potential use of the present method in detecting the expression of miRNA in the cells. The assay results show that the expression of miR-126 in MDA-MB231 cells is only ∼10% of that in MCF-10A cells (Figure 5; note that the expression of miR-126 in MDA-MB231 cells was normalized with that in MCF-10A cells), agreeing well with the previous report that miR-126 is a metastasis suppressor miRNA in human breast cancer and can reduce breast tumor growth.[9] These results indicate that the proposed assay method can also be used for estimating the miRNA expression in cells with good reliability.

In response to these previously reported methods for miRNA detection, our method operates via detecting the recovered fluorescence signal, which is a combined result of the specific hybridization and the site-specific endonuclease cleavage; thus, the detection should be relatively impervious to false signals arising due to the nonspecific adsorption of interferants. In addition to conventional methods and those newly emerging nanotechnology-based methods, our approach offers interesting possibilities to become a new and fast method for disease diagnosis. This novel approach could provide comprehensive and dependable information for the early detection of miRNA-related cancer.

CONCLUSIONS

In summary, we have described a new method for specifically detecting miRNA by coupling GO fluorescence quenching with site-specific cleavage of an endonuclease. The assay is based on the fluorescence recovery of the FAM-labeled probe, which was assembled on the GO surface, after it hybridized with the specific target (miR-126) and was cleaved by *Rsa*I endonuclease. The extraordinarily high quenching efficiency of GO and the high site-specific cleavage of *Rsa*I make the method a promising method for a miRNA assay with high sensitivity and selectivity. This assay can determine as low as ∼3.0 fM (at a signal/noise of 3) miR-126 with a linear range of 4 orders of magnitude and has an ability to discriminate the target sequence from even a single-base mismatched sequence and other miRNA sequences. In addition, the method can also be used for rapid estimation of the miR-126 expressions in several different types of cells. The advantage of this assay is that it is capable of functioning in complex samples and of avoiding false signals arising due to the nonspecific adsorption of interferants. This assay can be a potential tool for selective analysis of miRNAs (biomarkers) in tissues or cells, and it supplies valuable information for biomedical research and early clinical diagnosis.

ASSOCIATED CONTENT

Supporting Information

Additional information as noted in the text. This material is available free of charge via the Internet at http://pubs.acs.org.

AUTHOR INFORMATION

Corresponding Author

*E-mail: wuping@njnu.edu.cn (P.W.); cxcai@njnu.edu.cn (C.C.)

Notes

The authors declare no competing financial interest.

ACKNOWLEDGMENTS

This work is supported by the NSFC (21175067 and 21273117), the Research Fund for the Doctoral Program of Higher Education of China (20103207110004), the NSF of Jiangsu Province (BK2011779), the Foundation of the Jiangsu Education Committee (09KJA150001), the Program for Outstanding Innovation Research Team of Universities in Jiangsu Province, and the Priority Academic Program Development of Jiangsu Higher Education Institutions.

REFERENCES

(1) Aguda, B. D.; Kim, Y.; Piper-Hunter, M.; Friedman, A.; Marsh, C. B. *Proc. Natl. Acad. Sci. U.S.A.* **2008**, *105*, 19678−19683.
(2) Fabian, M. R.; Sonenberg, N.; Filipowicz, W. *Annu. Rev. Biochem.* **2010**, *79*, 351−379.
(3) Bartel, D. P. *Cell* **2004**, *116*, 281−297.
(4) Engels, B. M.; Hutvagner, G. *Oncogene* **2006**, *25*, 6163−6169.
(5) Plasterk, R. H. A. *Cell* **2006**, *124*, 877−881.
(6) Joglekar, M. V.; Joglekar, V. M.; Hardikar, A. A. *Gene Expression Patterns* **2009**, *9*, 109−113.
(7) O'Day, E.; Lal, A. *Breast Cancer Res.* **2010**, *12*, 201−210.
(8) Sun, Y.; Bai, Y.; Zhang, F.; Wang, Y.; Guo, Y.; Guo, L. *Biochem. Biophys. Res. Commun.* **2010**, *391*, 1483−1489.
(9) Tavazoie, S. F.; Alarcón, C.; Oskarsson, T.; Padua, D.; Wang, Q.; Bos, P. D.; Gerald, W. L.; Massagué, J. *Nature* **2008**, *451*, 147−152.
(10) Zhong, M.; Ma, X.; Sun, C.; Chen, L. *Chem.−Biol. Interact.* **2010**, *184*, 431−438.
(11) Mitchell, P. S.; Parkin, R. K.; Kroh, E. M.; Fritz, B. R.; Wyman, S. K.; Pogosova-Agadjanyan, E. L.; Peterson, A.; Noteboom, J.; O'Briant, K. C.; Allen, A.; Lin, D. W.; Urban, N.; Drescher, C. W.; Knudsen, B. S.; Stirewalt, D. L.; Gentleman, R.; Vessella, R. L.; Nelson, P. S.; Martin, D. B.; Tewari, M. *Proc. Natl. Acad. Sci. U.S.A.* **2008**, *105*, 10513−10518.
(12) Crawford, M.; Brawner, E.; Batte, K.; Yub, L.; Hunter, M. G.; Otterson, G. A.; Nuovo, G.; Marsh, C. B.; Nana-Sinkam, S. P. *Biochem. Biophys. Res. Commun.* **2008**, *373*, 607−612.
(13) Wang, X.-C.; Du, L.-Q.; Tian, L.-L.; Wu, H.-L.; Jiang, X.-Y.; Zhang, H.; Li, D.-G.; Wang, Y.-Y.; Wu, H.-Y.; She, Y.; Liu, Q.-F.; Fan, F.-Y.; Meng, A.-M. *Lung Cancer* **2011**, *72*, 92−99.
(14) Chang, J.; Nicolas, E.; Marks, D.; Sander, C.; Lerro, A.; Buendia, M. A.; Xu, C.; Mason, W. S.; Moloshok, T.; Bort, R.; Zaret, K. S.; Taylor, J. M. *RNA Biol.* **2004**, *1*, 106−113.
(15) Calin, G. A.; Croce, C. M. *Nat. Rev. Cancer* **2006**, *6*, 857−66.
(16) Young, D. D.; Connelly, C. M.; Grohmann, C.; Deiters, A. *J. Am. Chem. Soc.* **2010**, *132*, 7976−7981.
(17) Wark, A. W.; Lee, H. J.; Corn, R. M. *Angew. Chem., Int. Ed.* **2008**, *47*, 644−52.
(18) Pöhlmann, C.; Sprinzl, M. *Anal. Chem.* **2010**, *82*, 4434−4440.
(19) Zhang, Y.; Zhang, C. Y. *Anal. Chem.* **2012**, *84*, 224−231.
(20) Dodgson, B. J.; Mazouchi, A.; Wegman, D. W.; Gradinaru, C. C.; Krylov, S. N. *Anal. Chem.* **2012**, *84*, 5470−5474.
(21) Pall, G. S.; Codony-Servat, C.; Byrne, C. J.; Ritchie, L.; Hamilton, A. *Nucleic Acids Res.* **2007**, *35*, e60.
(22) Nelson, P. T.; Baldwin, D. A.; Scearce, L. M.; Oberholtzer, J. C.; Tobias, J. W.; Mourelatos, Z. *Nat. Methods* **2004**, *1*, 155−161.
(23) Li, J.; Yao, B.; Huang, H.; Wang, Z.; Sun, C. H.; Fan, Y.; Chang, Q.; Li, S. L.; Wang, X.; Xi, J. Z. *Anal. Chem.* **2009**, *81*, 5446−5451.
(24) Raymond, C. K.; Roberts, B. S.; Garrett-Engele, P.; Lim, L. P.; Johnson, J. M. *RNA* **2005**, *11*, 1737−1744.
(25) Persat, A.; Santiago, J. G. *Anal. Chem.* **2011**, *83*, 2310−2316.

(26) Varallyay, E.; Burgyan, J.; Havelda, Z. *Nat. Protoc.* **2008**, *3*, 190−196.
(27) Linsen, S. E. V.; de Wit, E.; Janssens, G.; Heater, S.; Chapman, L.; Parkin, R. K.; Fritz, B.; Wyman, S. K.; de Bruijn, E.; Voest, E. E.; Kuersten, S.; Tewari, M.; Cuppen, E. *Nat. Methods* **2009**, *6*, 474−476.
(28) Chen, C. F.; Ridzon, D. A.; Broomer, A. J.; Zhou, Z.; Lee, D. H.; Nguyen, J. T.; Barbisin, M.; Xu, N. L.; Mahuvakar, V. R.; Andersen, M. R.; Lao, K. Q.; Livak, K. J.; Guegler, K. J. *Nucleic Acids Res.* **2005**, *33*, e179.
(29) Yang, S. W.; Vosch, T. *Anal. Chem.* **2011**, *83*, 6935−6939.
(30) Liu, Y.-Q.; Zhang, M.; Yin, B.-C.; Ye, B.-C. *Anal. Chem.* **2012**, *84*, 5165−5169.
(31) Dong, H.; Zhang, J.; Ju, H.; Lu, H.; Wang, S.; Jin, S.; Hao, K.; Du, H.; Zhang, X. *Anal. Chem.* **2012**, *84*, 4587−4593.
(32) Peng, Y.; Gao, Z. *Anal. Chem.* **2011**, *83*, 820−827.
(33) Tu, Y.; Wu, P.; Zhang, H.; Cai, C. X. *Chem. Commun.* **2012**, *48*, 10718−10720.
(34) Li, Y.; Zhang, C.-Y. *Anal. Chem.* **2012**, *84*, 5097−5102.
(35) Lin, Y.; Tao, Y.; Pu, F.; Ren, J.; Qu, X. *Adv. Funct. Mater.* **2011**, *21*, 4565−4572.
(36) Qiao, G.; Gao, Y.; Li, N.; Yu, Z.; Zhuo, L.; Tang, B. *Chem.—Eur. J.* **2011**, *17*, 11210−11215.
(37) Fan, Q.; Zhao, J.; Li, H.; Zhu, L.; Li, G. *Biosens. Bioelectron.* **2012**, *33*, 211−215.
(38) Lynn, S. P.; Cohen, L. K.; Kaplan, S.; Gardner, J. F. *J. Bacteriol.* **1980**, *142*, 380−383.
(39) Hummers, W. S.; Offeman, R. E. *J. Am. Chem. Soc.* **1958**, *80*, 1339−1339.
(40) Kovtyukhova, N. I.; Ollivier, P. J.; Martin, B. R.; Mallouk, T. E.; Chizhik, S. A.; Buzaneva, E. V.; Gorchinskiy, A. D. *Chem. Mater.* **1999**, *11*, 771−778.
(41) Wu, X.; Hu, Y.; Jin, J.; Zhou, N.; Wu, P.; Zhang, H.; Cai, C. X. *Anal. Chem.* **2010**, *82*, 3588−3596.
(42) Hu, Y. J.; Wu, P.; Yin, Y. J.; Zhang, H.; Cai, C. X. *Appl. Catal., B* **2012**, *111−112*, 208−217.
(43) Wu, P.; Qian, Y.; Du, P.; Zhang, H.; Cai, C. X. *J. Mater. Chem.* **2012**, *22*, 6402−6412.
(44) Shao, Q.; Wu, P.; Xu, X.; Zhang, H.; Cai, C. X. *Phys. Chem. Chem. Phys.* **2012**, *14*, 9076−9085.
(45) Sambrook, J.; Fritsch, E. F.; Maniatis, T. *Molecular Cloning, A Laboratory Manual*, 2nd ed.; Cold Spring Harbor Laboratory Press: Cold Spring Harbor, NY, 1989.
(46) Liu, X.; Aizen, R.; Freeman, R.; Yehezkli, O.; Willner, I. *ACS Nano* **2012**, *6*, 3553−3563.
(47) Lu, C.-H.; Yang, H.-H.; Zhu, C.-L.; Chen, X.; Chen, G.-N. *Angew. Chem., Int. Ed.* **2009**, *48*, 4785−4787.
(48) He, S.; Song, B.; Li, D.; Zhu, C.; Qi, W.; Wen, Y.; Wang, L.; Song, S.; Fang, H.; Fan, C. *Adv. Funct. Mater.* **2010**, *20*, 453−459.
(49) Lee, J.; Kim, Y.-K.; Min, D.-H. *Anal. Chem.* **2011**, *83*, 8906−8912.
(50) Zhao, J.; Chen, G.; Zhu, L.; Li, G. *Chem. Commun.* **2011**, *13*, 31−33.
(51) Li, Z.-Y.; Xi, Y.; Zhu, W.-N.; Zeng, C.; Zhang, Z.-Q.; Guo, Z.-C.; Hao, D.-L.; Liu, G.; Feng, L.; Chen, H.-Z.; Chen, F.; Lv, X.; Liu, D.-P.; Liang, C.-C. *J. Hepatol.* **2011**, *55*, 602−611.